Subtle competition between ferromagnetic and antiferromagnetic order in a Mn(II) - free radical ferrimagnetic chain

E. Lhotel,[1] V. Simonet,[2,*] E. Ressouche,[3] B. Canals,[2] D. B. Amabilino,[4] C. Sporer,[4] D. Luneau,[5] J. Veciana,[4] and C. Paulsen[1]

[1] *Centre de Recherche sur les Très Basses Températures, CNRS, BP 166, 38042 Grenoble, France*
[2] *Laboratoire Louis Néel, CNRS, BP 166, 38042 Grenoble, France*
[3] *CEA-Grenoble, DRFMC / SPSMS / MDN, 17 rue des Martyrs, F-38054 Grenoble cedex, France*
[4] *Institut de Ciència de Materials de Barcelona (CSIC), Campus Universitari, 08193 Bellaterra, Spain*
[5] *Université Claude Bernard-Lyon 1, Laboratoire des Multimatéraiux et Interfaces (UMR 5615), Bât Raulin - Campus de la Doua, 69622 Villeurbanne Cedex, France*

The macroscopic magnetic characterization of the Mn(II) - nitronyl nitroxide free radical chain ($Mn(hfac)_2(R)$-3MLNN) evidenced its transition from a 1-dimensional behavior of ferrimagnetic chains to a 3-dimensional ferromagnetic long range order below 3 K. Neutron diffraction experiments, performed on a single crystal around the transition temperature, led to a different conclusion : the magnetic Bragg reflections detected below 3 K correspond to a canted antiferromagnet where the magnetic moments are mainly oriented along the chain axis. Surprisingly in the context of other compounds in this family of magnets, the interchain coupling is antiferromagnetic. This state is shown to be very fragile since a ferromagnetic interchain arrangement is recovered in a weak magnetic field. This peculiar behavior might be explained by the competition between dipolar interaction, shown to be responsible for the antiferromagnetic long range order below 3 K, and exchange interaction, the balance between these interactions being driven by the strong intrachain spin correlations. More generally, this study underlines the need, in this kind of molecular compounds, to go beyond macroscopic magnetization measurements.

PACS numbers: 75.50.Xx, 75.25.+z, 75.10.Pq

I. INTRODUCTION

The organic chemistry synthesis approach, applied in the field of molecular magnetism, has allowed to obtain original compounds with properties characteristic of both classical magnets and organic compounds. Some of the early successes reported in this field were the finding of a purely organic ferromagnet[1], the experimental proof of the Haldane conjecture in a molecular chain compound[2], or the study of single molecule magnets providing model systems for the investigation of quantum effects such as quantum tunneling of magnetization or topological interferences[3,4].

Another important achievement was made in the field of molecular magnetic one-dimensional (1D) compounds with the design of ferrimagnetic chain compounds. They consist of magnetically quasi-isolated chains where two kinds of different magnetic centers alternate regularly. The first example was identified in a bimetallic ferrimagnetic chain compound[5] built of Mn^{2+} ions with spin 5/2 and Cu^{2+} ones with spin 1/2. Several other types of ferrimagnetic chains were then discovered with various metallic centers, different spatial intra and interchain architectures, alternating interaction pathways within the chains, leading to different magnetic properties especially at low temperature where interchain interactions begin to play a role[6]. Not only bimetallic materials but also metallo-organic chains, in which the spin carriers are a metallic ion and an organic free radical, generally nitroxide, were synthesized and proved to enrich further the variety of magnetic behaviors[6,7,8,9,10,11,12]. Very recently, this kind of materials was reinvestigated with new questions concerning in particular the nature of the slow spin dynamics in Ising like chain compounds[13,14,15]. The slow relaxation of magnetization, in first order agreement with the theory of Glauber concerning Ising 1D chain[16], is a consequence of strong uniaxial anisotropy and also of intrachain magnetic correlations.

The success of the metallo-organic route chosen by several groups hold on the use of nitronyl nitroxide free radicals (NITR) where R stands for an alkyl or aromatic group. This organic entity has one unpaired electron carrying a spin 1/2, delocalized on the 5 atoms of its O-N-C-N-O fragment as shown by polarized neutron studies on a compound of very weakly interacting nitronyl nitroxide molecules[17]. This original electronic configuration allows the radical to be coupled simultaneously to two metallic groups. These groups can be built of one magnetic 3d metallic ion M like Cu, Ni, Mn or Co, surrounded by magnetic inactive bulky organic moieties like hexafluoroacetylacetonates (hfac)[7,8,9,10,12,18]. The use of this NITR free radical leads preferentially to antiferromagnetic intrachain coupling stronger than in bimetallic ferrimagnetic chain compounds, except in the case of some Cu complexes where it is ferromagnetic. The possible cis or trans NITR-$M(hfac)_2$ coordination scheme, determined by the R group, can produce different architectural arrangements leading to linear, zig-zag or helical chains with different magnetic properties. These were studied by Caneschi *et al.*[9] within the rich family of the Mn-NITR compounds. Several compounds with different R group, studied by magnetometry and EPR, were

shown to present a ferrimagnetic 1D behaviour. At low temperature, between 5 and 9 K, they undergo a transition towards a three-dimensional (3D) long-range order (LRO) consisting of a ferromagnetic ordering of the Mn-NITR entities.

In these materials, chains are well magnetically isolated from each other thanks to their large separation by bulky magnetically inactive organic moieties. This results in very weak interchain exchange interactions, leading to a ratio of intra to interchain interaction that reaches several orders of magnitude and a strong 1D behaviour. Then it is necessary to take into account other usually neglected interactions such as the dipolar one. In pure 1D compound, LRO is not expected at finite temperature, but very weak interchain dipolar interactions, reinforced by strong intrachain correlations, can induce such a 3D LRO[19,20,21]. The role of dipolar interaction is also invoked to explain the 3D magnetic ordering of high spin molecular cluster compounds[22,23].

The present studied chain compound[18], $Mn(hfac)_2(R)$-3MLNN with the NITR free radical (R)-3MLNN=(R)-Methyl[3-(4,4,5,5-tetramethyl-4,5-dihydro-1*H*-imidazolyl-1-oxy-3-oxide) phenoxy]-2-propionate, shown in Fig. 1, is formed by alternating Mn^{2+} ions carrying a spin 5/2 and chiral nitronyl nitroxide free radicals. It crystallizes in the non-centrosymmetric orthorhombic $P2_12_12_1$ space group. There are 4 formulas $C_{27}H_{25}F_{12}Mn_2O_9$ per unit cell which sum up to 304 atoms. The Mn^{2+} ions are in the center of a distorted oxygen octahedron, linked to two hfac moieties and two NITR radicals in cis coordination which gives the compound its zig-zag structure. The resulting chains propagate along the b axis with Mn-Mn distances of 7.57 Å within the chains and of at least 11.3 Å between adjacent chains. Each chain is surrounded by 6 others, some of those related by a screw axis.

The possibility to work with a $Mn(hfac)_2(R)$-3MLNN single-crystal, sufficiently stable for neutron diffraction measurements, allowed us for the first time in this kind of metallo-organic ferrimagnetic chain, to determine unambiguously the nature of the 3D LRO stabilized at low temperature and to evidence strong magnetic competition. A first magnetic investigation of this compound by macroscopic measurements was reported in Ref. 18, and is recalled in section II. The determination by neutron diffraction of the magnetic LRO below the transition is presented in section III.1. Since it can not be explained with the same kind of magnetic interaction than the correlations probed by magnetic measurements, a neutron diffraction experiment under a magnetic field was further performed (cf. section III.2) that showed the low robustness of the LRO state versus a very small field. Those results are discussed in terms of competing interactions in section IV.

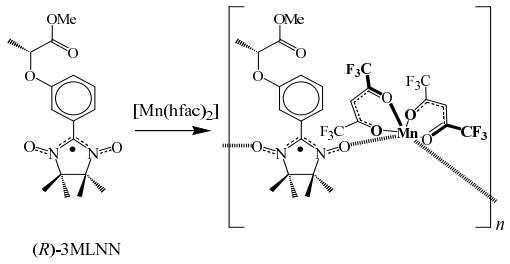

FIG. 1: Schematic representation of the $(Mn(hfac)_2(R)$-3MLNN complex.

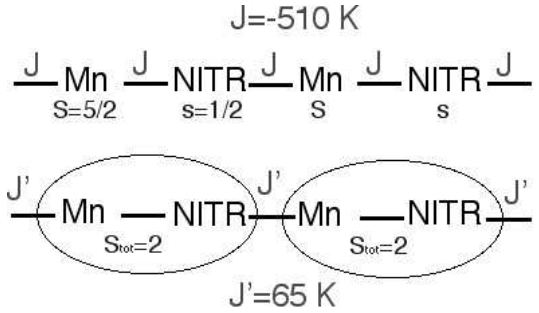

FIG. 2: Schematic representation of the intrachain interactions J and J'.

II. MAGNETIZATION MEASUREMENTS

The macroscopic magnetic properties of $Mn(hfac)_2(R)$-3MLNN single-crystals were investigated by dc magnetization and ac susceptibility measurements using three superconducting quantum interference device (SQUID) magnetometers. One is commercial (0-80 kOe, 2-200 K). The two others, developed at the CRTBT/CNRS, are equipped with a miniature dilution refrigerator: one is devoted to low field measurements (0-2 kOe), and the second to high field (0-80 kOe).

Measurements in the three directions have shown that there is a weak uniaxial anisotropy along the chain direction (b axis). The anisotropy constant $K \approx 2.5 \times 10^3$ J.m^{-3} was estimated from saturation magnetization and perpendicular susceptibility measurements at low temperatures. Hereafter, we will focus on measurements performed along the easy axis.

The high temperature characterization of the sample was made by magnetization measurements in a field of H_{dc}=10 Oe from T=20-90 K and by AC susceptibility measurements in a field H_{ac}=1.4 Oe from T=5-20 K. Throughout these temperature ranges, the fields are small enough to ensure that the magnetization is linear in field, so that the magnetization M/H equals the linear susceptibility χ.

A 1D ferrimagnetic behavior expected from the non-compensation of the Mn^{2+} isotropic spins S=5/2 and the NITR free radical spins s=1/2 is observed above

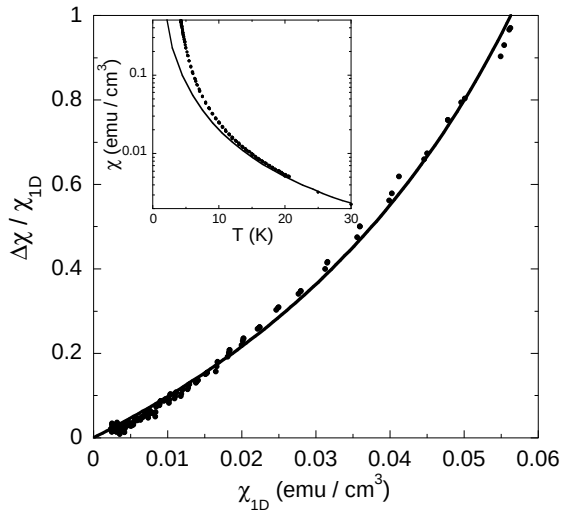

FIG. 3: $\Delta\chi/\chi_{1D}$ *vs.* χ_{1D} (see text) for 5 $K < T < 20$ K. The line is a fit to Eq. 2 with J_{inter}/k_B =4.3 mK. The inset shows the measured χ *vs.* T (dots) and its departure from the calculated one (line) for a 1D behavior (Eq. 1) below 20 K.

20 K[18]. The high temperature magnetic susceptibility is indeed compatible with a strong antiferromagnetic coupling J/k_B=-510 K between the Mn and the NITR spins inside the chains[24,25] which is not broken even at room temperature[18]. Therefore, at lower temperature (below 100 K), the chains can be considered as S_{tot}=S-s=2 effective units, ferromagnetically coupled by an exchange J' as represented in Fig. 2. Between 20 and 90 K ($J'S_{tot}^2/k_BT \gg 1$), the susceptibility χ(T) can then be fitted in the framework of 1D ferromagnetic chains[26] by Eq. 1. The fit yields J'/k_B=65 K.

$$20\ K < T < 90\ K, \quad \chi = \chi_{1D} = \alpha \frac{2}{3J'} \left(\frac{J'S_{tot}^2}{k_B T} \right)^2 \quad (1)$$

with $\alpha = ng^2\mu_B^2$, where n is the number of magnetic entities and setting g=2 (value obtained by EPR measurements[27]) .

Below 20 K, we observe deviations from the 1D susceptibility χ_{1D}(T) extrapolated using the J' value deduced above 20 K (see the inset of Fig. 3). This feature announces a crossover from high temperature 1D to 3D short-range correlations. The positive difference of $\Delta\chi = \chi - \chi_{1D}$ indicates the presence of ferromagnetic interactions between the chains. We can estimate these interactions from a mean-field approach with the equation[28]:

$$5\ K < T < 20\ K, \qquad \frac{\Delta\chi}{\chi_{1D}} = \frac{zJ_{inter}\chi_{1D}/\alpha}{1 - zJ_{inter}\chi_{1D}/\alpha} \quad (2)$$

where $z = 6$ is the number of first neighbor chains and J_{inter} is the total interchain exchange interaction. Note that demagnetization effects are negligible in this temperature range. The fit between 5 and 20 K, shown in Fig. 3, leads to $J_{inter}/k_B \approx 4$ mK, which confirms the strong 1D character of the system: $J_{intra}/J_{inter} > 10^4$.

When the temperature is further decreased, the Mn-radical chain has been shown to undergo a magnetic transition at T_c=3 K[18]. Our analysis of the susceptibility above T_c reveals a small ferromagnetic interchain interaction and in addition, at T_c, the susceptibility exhibits a large peak with a magnitude equal to the inverse of the demagnetizing factor N, within the error bars in the determination of N. As a result of these observations, the transition was at first attributed to ferromagnetic LRO[18].

Indeed, below T_c and in moderated to strong magnetic fields, the field dependence of the magnetization seems to be well accounted for by a classical ferromagnetic order. In the high field regime, magnetization curves saturate rapidly as seen in top Fig. 4, although they do not reach the expected total saturation value until 80 kOe. In fact, the curves show a non zero slope which is characteristic of the presence of a small canting, estimated to be of the order of 10° with respect to the b axis. At low fields, but larger than 5 Oe, the magnetization curves seem to vary linearly with the field, with a slope dM/dH approximately equal to the inverse of the demagnetizing factor (see bottom Fig. 4). In addition, below 2.5 K the ac susceptibility is frequency dependent and presents thermomagnetic irreversibilities, and below 1 K magnetic hysteresis loops appear as previously reported[18]. These properties are reminiscent of ferromagnetic behavior in the presence of pinning and depinning of domain-walls, and therefore in agreement with the hypothesis of a canted ferromagnetic order stabilized in this system.

However, an intriguing behavior is observed for very low fields, H<5 Oe, where the M(H) curves exhibit a negative curvature (see the curve at 1.8 K in the inset of the bottom Fig. 4). Furthermore, the spontaneous magnetization could not be extracted from the magnetization curves, or from Arrott plots[29] of the data. The inconsistency in the results, apparent ferromagnetic behavior without a spontaneous magnetic moment, suggests that a nonconventional LRO is taking place. This was the motivation for neutron diffraction measurements in order to determine the actual magnetic structure of the Mn(hfac)$_2$(R)-3MLNN compound below T_c.

III. NEUTRON DIFFRACTION EXPERIMENTS

The experiments were performed on the two CRG thermal-neutron single-crystal diffractometers, D15 and D23, at the Institut-Laue-Langevin high flux reactor (ILL, Grenoble, France). Both diffractometers were operated in normal-beam mode, using an incident wavelength of 1.1694 and 1.2582 Å for D15 and D23 respectively. The D15 experiment was aimed at determining the nuclear and magnetic structures in zero magnetic field in the 1.5-10 K temperature range around T_c. The D23

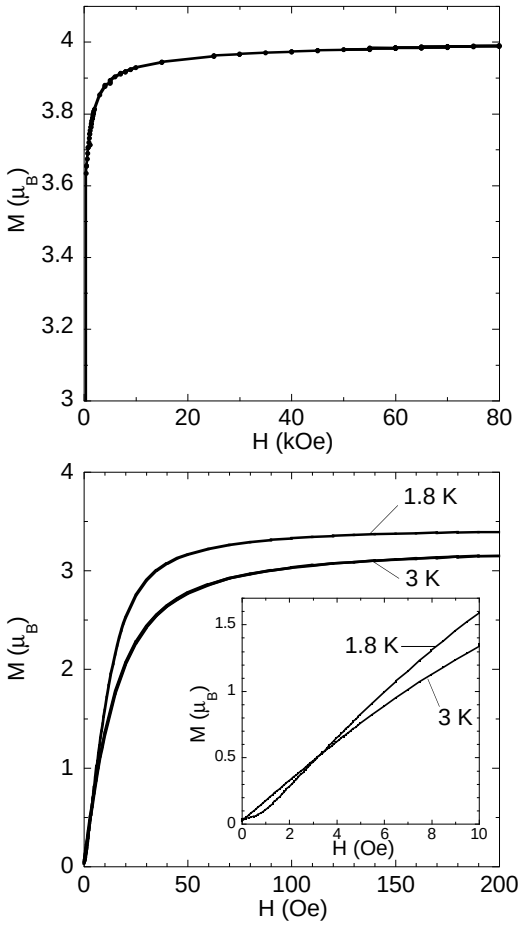

FIG. 4: *M vs. H* at 200 mK up to 80 kOe (top) ; at 1.8 *K* and 3 *K* up to 200 Oe (bottom) with a zoom in the very small magnetic field range in the inset.

experiment yielded information about the evolution of the magnetic structure under magnetic field and was performed using a vertical cryomagnet (6 T superconducting coil).

The sample was a very small crystal of $Mn(hfac)_2(R)$-3MLNN of $\approx$ 4.4 mg and 1 mm^3 which was held in a thin Al box with apiezon grease and positioned with the *b* axis vertical on the spectrometer. This set-up was chosen instead of direct gluing due to the brittleness of the sample, also very sensitive to temperature cycling.

A. Nuclear structure

The first step of the neutron diffraction experiment consisted in refining the low temperature nuclear structure, previously determined from X-ray diffraction at room temperature with calculated H positions. The X-ray structure obtained with a Rf factor of 19% suggested the presence of some disorder[18]. For the neutron refinement purpose, 352 Bragg reflections were collected on D15 at 10 K. Unfortunately it was impossible to collect more reflections because of the fast deterioration of the sample upon temperature cycling. The resulting lattice parameters are a=11.84, b=13.79, c=20.03 Å. The integrated intensities corrected from the Lorentz factor were calculated from the ω-scans with the COLL5 program[30]. The averaging of the equivalent reflections and absorption correction were done using the ARRNGE and AVEXAR programs from the CCSL library[31] with an estimated total absorption coefficient μ of 0.12 mm^{-1}, essentially due to the large incoherent scattering of the hydrogen atoms. The weakness of the measured signal, the presence of important structural disorder, and the small number of collected Bragg reflections imposed a limit to the number of free parameters in the refinement procedure.

This was achieved using a method based on rigid molecular blocks. A new implementation in the MXD program[32] was used to handle this by adjusting, for each block of atoms, the 3 coordinates of its origin, and the 3 eularian angles parameterizing its three dimensional rotation around this point. 3 main blocks were chosen on chemical grounds : the block associated to the NITR radical had free origin coordinates and free rotation angles whereas the two hfac blocks had a fixed origin with respect to the Mn, only the rotation angles being free in the refinement. 13 minor groups (shown in Fig. 5) were further selected within these main blocks, which were allowed to rotate around the parent C-C or C-O bond axis: 4 CF_3 groups within the hfac blocks, 5 methyl groups, 1 phenyl group and the 4 segments of the carbonate chain linked to the phenyl within the NITR block. Including one isotropic thermal factor for each kind of chemical species, this led us to fit the measured intensities with 36 refinable variables for 358 observations. The resulting structure, obtained with a weighted Least Square R factor of 13.2 % (see Fig. 6), presents slight modifications with respect to the published structure[18], consisting essentially of rigid block rotation angle deviation of 5.3° at most. This treatment provided us with a determination of the positions of the magnetic atoms and of the scaling factor necessary for a quantitative analysis of the magnetic structure.

B. Magnetic structure in zero field

A weak magnetic signal was observed at 1.5 K on top of some nuclear peaks from the difference with the 10 K measurements and on the (*h*,0,0) and (0,0,*l*) reflections with odd *h* and *l* indices. Those reflections, absent in the nuclear pattern, are forbidden in this space group due to point group symmetries relating the 4 asymmetric units. These observations for such a non-Bravais lattice imply a $\boldsymbol{k}$=0 propagation vector with an antiferromagnetic arrangement of the 4 magnetic entities per unit cell.

In order to check the intrinsic origin of the observed magnetic Bragg peaks, the intensity at the peak maximum position for the purely magnetic (-1,0,0) reflection,

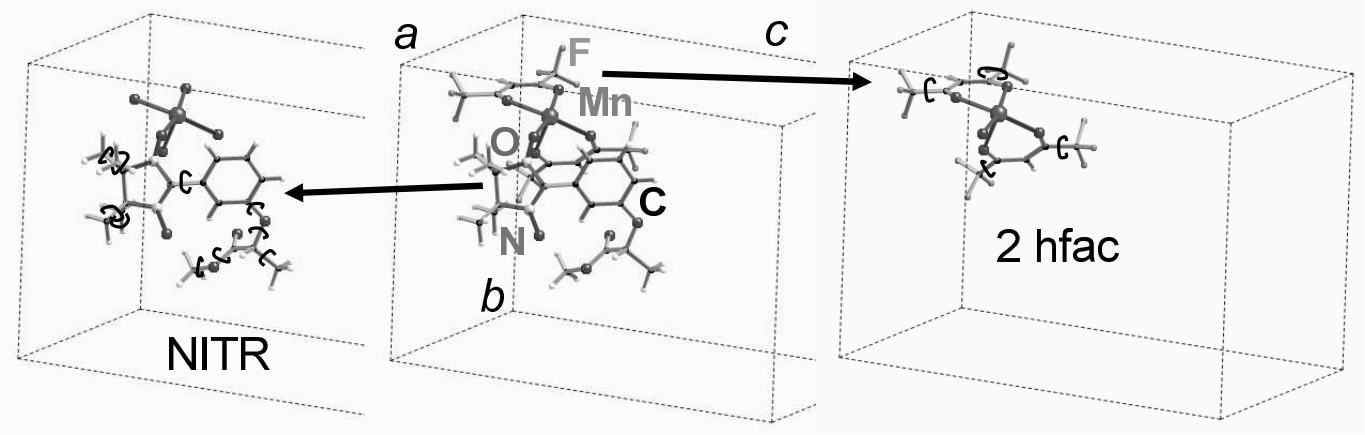

FIG. 5: Representation of the 13 rigid molecular blocks within the main NITR and hfac blocks allowed to rotate (black signs around the rotation axis bond) in the nuclear structure refinement (see text).

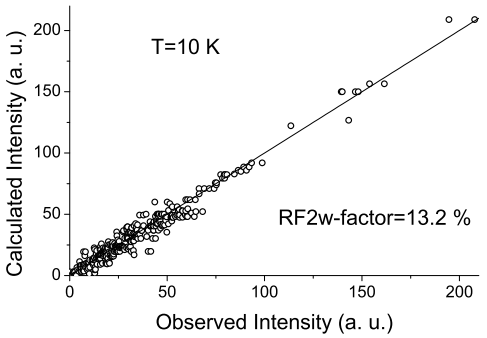

FIG. 6: Graphical representation of the $Mn(hfac)_2(R)$-3MLNN nuclear structure refinement at 10 K : calculated versus measured integrated intensities.

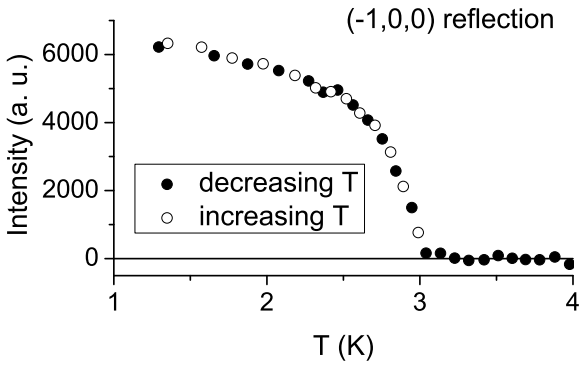

FIG. 7: Temperature variation of the magnetic signal associated to the (-1,0,0) reflection : neutron counts at the peak maximum corrected from the 2.5° ω-shifted background. The error bars are smaller than the symbol size.

characteristic of antiferromagnetic LRO, was followed with increasing and decreasing temperature, as shown in Fig. 7. The signal vanishes at 3 K in agreement with the transition temperature deduced from the susceptibility measurements. Note the presence of a small kink in the magnetization versus temperature around 2.4 K. Although the origin of this slight change of magnetization is unclear, it should be noted that this temperature coincides with the onset of a non trivial dynamical magnetic behaviour recorded in the ac susceptibility measurements[18].

The analysis of the magnetic signal was made using the differences between the 1.5 K and 10 K intensities of 52 reflections including a set of (h,0,0) and (0,0,l) reflections with odd h and l indices. For these special reflections, the magnetic signal was directly deduced from the integration of 10 mn/point ω-scans. Due to the weakness of the magnetic signal compared to the nuclear one, for the mixed nuclear and magnetic reflections, the magnetic signal was obtained from the difference between 21 mn neutron counts at the peak maximum position corrected from the side background, measured at 10 and 1.5 K. The difference was then renormalized by the integrated intensity of a 3 mn/point ω-scan.

To simplify the analysis, group theory can be used in order to predict the possible magnetic arrangements compatible with the crystal symmetries and as a consequence to reduce the number of independent parameters in the refinement procedure. In the Landau theory, the magnetic fluctuations in the paramagnetic state reflect the crystal symmetries. At a second-order phase transition, one of the modes is stabilized. Each mode corresponds to one irreducible representation of the symmetry group Gk that leaves the propagation vector $\boldsymbol{k}$ invariant. The application of the Group theory to the present

	τ^1	τ^2	τ^3	τ^4
Mn	1 2 3 4	1 2 3 4	1 2 3 4	1 2 3 4
m_x	+ - + -	+ + + +	+ + - -	+ - - +
m_y	+ - - +	+ + - -	+ + + +	+ - + -
m_z	+ + - -	+ - - +	+ - + -	+ + + +

TABLE I: Magnetic components for the 4 Mn atoms : Mn_1 (0.400, 0.189, 0.267), Mn_2 (0.100, 0.811, 0.767), Mn_3 (0.900, 0.311, 0.733) and Mn_4 (0.600, 0.689, 0.233) for each irreducible representations τ^1, τ^2, τ^3 and τ^4.

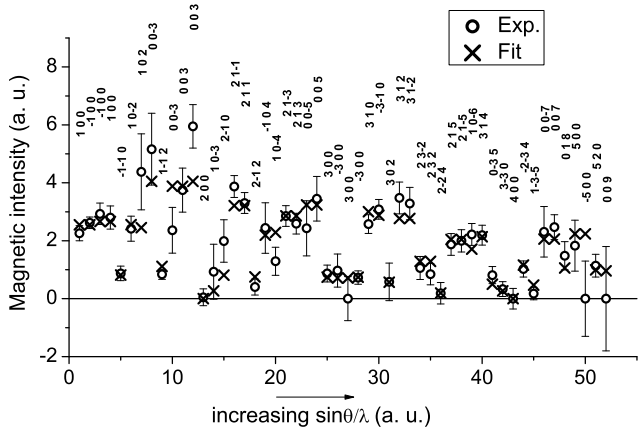

FIG. 8: Least square refinement of the magnetic structure in zero field at 1.6 K: comparison of the measured and calculated integrated intensities for the top labeled reflections displayed with increasing $sin(\theta)/\lambda$.

crystal, using the tabulated irreducible representations by Kovalev[33], shows that the group representation can be reduced to a sum of 4 irreducible representations of order 1 : $\Gamma = 3\tau^1 \oplus 3\tau^2 \oplus 3\tau^3 \oplus 3\tau^4$. The 4 possible magnetic arrangements deduced from this analysis are summarized in Table I.

It is interesting to notice that the presence of a magnetic signal on the (h,0,0) and (0,0,l) Bragg positions with odd h and l allows to distinguish between these four magnetic structures. τ^1 is the only representation predicting a magnetic signal on both (h,0,0) and (0,0,l) reflections. The τ^3 representation yields no signal on both types of reflections. In the case of τ^2, a magnetic signal is expected on the (h,0,0) reflections and not on the (0,0,l) ones, and the inverse is predicted for the τ^4 representation. For the present measurements, the magnetic signal observed at 1.5 K on the (h,0,0) reflections with h=1,3,5 and on the (0,0,l) reflections with l=3,5,7 therefore suggests a magnetic arrangement associated with the τ^1 representation.

The above representation analysis was carried out by considering spins at the Mn positions only. However, a correct treatment of the neutron data must in addition properly include the smaller delocalized moment of the NITR free radicals which is strongly antiferromagnetically coupled to the Mn one. If the distribution of the magnetization (or form factor) around a Mn ion is well known and tabulated, the major difficulty of evaluating the radical contribution comes from the extended nature of the spin distribution on this organic fragment. The magnetization distribution in a quasi-isolated phenyl-substituted nytronil nitroxide free radical was measured using polarized neutron[17]. This work showed that, in such a radical, most of the spin density is found equally shared between the 4 atoms of the two NO groups of the nitronyl nitroxide. An additional negative contribution, due to the spin polarization effect, is also observed on the central C atom. This picture has been used to model the spin distribution on the nitronyl nitroxide in the present case and to deduce a "pseudo" form factor that enters the expression of the intensity of a magnetic reflection. In practice, the magnetic structure factor was obtained at each scattering vector $\boldsymbol{Q}$ by summing the contributions of the 4 Mn and the 4 NITR of the asymmetric unit, as in Eq. 3. In this equation, $f_{Mn}(Q)$ and $\boldsymbol{m}^j_{Mn}$ are respectively the magnetic form factor and the magnetic moments for each Mn and $p = 0.2696 \times 10^{-12}$ cm. $\boldsymbol{m}^j_{NITR}$ is the magnetic moment carried by the free radical whereas $(a_j + ib_j)$ is a complex number evaluated at each measured (h,k,l) reflection that represents both the "pseudo" form factor and the geometrical term arising from the positions of the 5 atoms O, N, C, N and O that are known to carry the spin in the radical.

$$\boldsymbol{F}_M(\boldsymbol{Q}) = p\sum_{j=1}^{4}[f_{Mn}(Q)\boldsymbol{m}^j_{Mn}\exp(i\boldsymbol{Q}.\boldsymbol{r}_j) + \boldsymbol{m}^j_{NITR}(a_j + ib_j)] \quad (3)$$

Note that a strong exchange interaction between the NITR and the metallic centers can modify the spin distribution determined in Ref. 17,34. In our case this should only slightly affect the quantitative results we have obtained.

The final least-square refinement of the magnetic integrated intensities with the τ^1 representation for both Mn and NITR radical was then performed. Note that the three other representations yielded worse results (χ^2=2.28, 2.05, 1.58 for τ^2, τ^3 and τ^4 respectively) as expected from the absence of magnetic signal on (h,0,0) and/or (0,0,l) Bragg positions. The fit is also improved with respect to a calculation with only an effective spin at the Mn position (χ^2=2.03). The best agreement (see Fig. 8 and Table II) obtained with a reduced χ^2 factor of 1.03 corresponds to a canted antiferromagnetic structure (see Fig. 9). Within the chain, the main direction for the Mn^{2+} moments is along the b axis, m_y=4.07±0.08 μ_B, with small antiferromagnetic components along the a and c axis : m_x=1±0.7 μ_B and m_z=-0.7±0.5 μ_B. The corresponding tilt angle with respect to the b axis is roughly equal to 16°. There is a large uncertainty concerning the exact orientation of the NITR moment but its main

	x	y	z	M_x	M_y	M_z
Mn_1	0.400	0.189	0.267	1.0	4.07	-0.7
Mn_2	0.100	0.811	0.767	-1.0	-4.07	-0.7
Mn_3	0.900	0.311	0.733	1.0	-4.07	0.7
Mn_4	0.600	0.689	0.233	-1.0	4.07	0.7
$NITR_1$	0.480	0.440	0.230	0	-0.7	0
$NITR_2$	0.020	0.560	0.730	0	0.7	0
$NITR_3$	0.980	0.060	0.770	0	0.7	0
$NITR_4$	0.520	0.940	0.270	0	-0.7	0

TABLE II: Magnetic structure of $Mn(hfac)_2(R)$-3MLNN in zero magnetic field at 1.5 K, refined assuming the NITR moment to be parallel to the b axis. The atomic coordinates and components of the magnetic moments (in μ_B) are given for the 4 Mn and NITR of the asymmetric unit. For the NITR, the average magnetic moment is defined as in Eq. 3 and the atomic coordinates are those of the central carbon atom of the O-N-C-N-O fragment carrying most of the spin density. The magnetic moment error bars are 0.7, 0.08 and 0.5 μ_B for the 3 components of the Mn and 0.1 μ_B for the NITR y component.

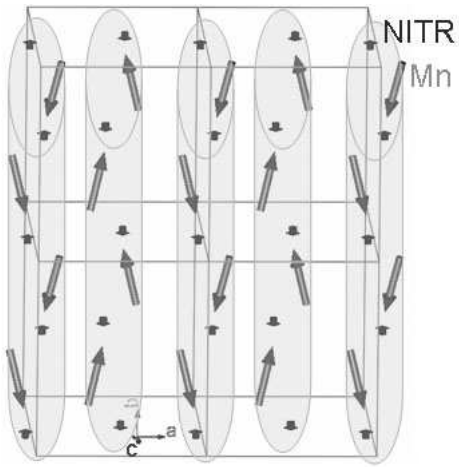

FIG. 9: Schematic representation of the magnetic structure at 1.5 K and zero magnetic field. The long and short arrows represent the Mn and NITR moments respectively.

component is along the chain axis, antiparallel to the Mn one. Constraining the NITR moment to lie along the b axis yields a moment component of m_y=-0.7±0.1 μ_B. Note that both Mn (4.25±0.3 μ_B) and NITR (0.7±0.1μ_B) moments have slightly reduced values. This could be associated to some deterioration of the crystal or to a delocalization of the NITR spin density on the Mn site. Finally, the interchain coupling between the two chains of the unit cell is found antiferromagnetic. The structure can then be described as slightly canted ferromagnetic (a, b) sheets, antiferromagnetically stacked along the c direction with a ($a/2$, $b/2$) translation.

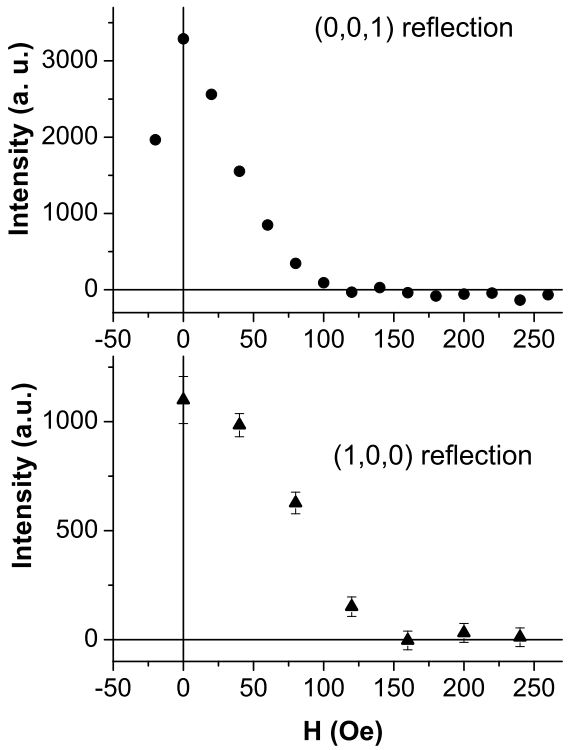

FIG. 10: Variation with magnetic field of the magnetic signal associated to the (-1,0,0) and (1,0,0) reflections at 1.6 K : neutron counts at the maximum peak position corrected from the background. The error bars are within the symbol size for the (0,0,1) reflection.

C. Evolution with a magnetic field

The antiferromagnetic structure under zero field described in the previous section is a surprising result, in apparent contradiction with the magnetization and susceptibility measurements. This motivated a subsequent neutron scattering experiment performed on the D23 spectrometer during which the robustness of the magnetic structure determined in zero field was tested under a magnetic field applied parallel to the b axis. A few peaks, in particular the (h,0,0) and (0,0,l) ones with odd indices, characteristic of the antiferromagnetic arrangement, were followed under a magnetic field at 1.6 K.

The presence of the magnetic arrangement associated to the τ^1 representation was first confirmed by the rise of magnetic signal observed on the (0,0,3), (0,0,1) and (1,0,0) reflections between 5 and 1.6 K in zero field. At 1.6 K, the magnetic intensities recorded on the (1,0,0) and (0,0,1) reflections were then measured while varying the field and shown to be wiped out very rapidly : A small field of the order of 100 to 150 Oe is sufficient to completely kill these magnetic reflections (see Figs.

10). Note that a small hysteresis was observed ($\sim$ 30 Oe shift), maybe due to the lack of precision of the 6 T magnet in this range of applied fields. Although the full evolution of the magnetic structure under a magnetic field was not measured, the persistence of a magnetic signal at a field H_c sufficient to cancel the (0,0,l) and (h,0,0) reflections was checked. This was achieved by measuring the difference between the integrated intensities at 5 K in zero field and at 1.6 K in H_c on both (-2,1,0) and (1,0,-4) reflections. The magnetic signal is significantly reduced on (1,0,-4) and increased on (-2,1,0) when applying the field. This is in agreement with the expected field-induced transition towards a ferromagnetic interchain arrangement of the moments (τ^3 representation), possibly slightly canted although the accuracy of the measurement is not sufficient to quantify this point.

IV. DISCUSSION

The antiferromagnetic LRO determined by neutron diffraction below T_c is therefore different from the one expected through the observation at higher temperatures of 3D ferromagnetic correlations. It is furthermore very easily destabilized under a weak magnetic field. To interpret this behavior, we will consider in the following the magnetic couplings that are effective in this temperature range, and in particular their interchain contribution, as a necessary ingredient to drive the system to a 3D LRO.

A good candidate for this interchain mechanism, often invoked in chain compounds[9,19,20,21], is the weak but long-ranged dipolar coupling. In addition to its role in the onset of 3D LRO, the dipolar interaction is also argued to be responsible for the magnetic anisotropy observed in some Mn-based chain compounds[9,19]. The importance of dipolar anisotropy is a consequence of the weakness of the single-ion anisotropy, describable as a crystal zero field splitting of the ion ground state. For Mn^{2+}, there is no zero-field splitting in 1^{st} order of perturbation due to the zero orbital angular momentum of its $^6S_{5/2}$ ground state. Non-zero values can only arise from higher order processes allowing the interaction of the ions with the crystal field, the most important mechanism being the admixtures through spin-orbit coupling of $L \neq 0$ excited states within the ground state[35]. In the present Mn-NITR chain compound, we observe a weak axial anisotropy of the magnetic moments. They are mainly oriented along the chain axis, with a small canting. Such a magnetic orientation appears to be rare in spin chains where the moments usually lie perpendicular to the chain axis. This perpendicular orientation is expected for systems consisted of an antiferromagnetic stacking of spins along the chain axis in which the dipolar interaction is the main source of anisotropy. The origin of the anisotropy in the present case where the magnetic entities are Mn^{2+} and organic radicals with isotropic spins 1/2 is therefore questionable.

In order to check the role of dipolar coupling in the orientation of the spins and in the onset of a finite temperature LRO, we have used a mean field (MF) approach. The method is only briefly described in this paper but more details about the formalism may be found for instance in Ref. 36. We have used a general anisotropic Hamiltonian which takes into account the intrachain isotropic exchange couplings ($J = -510$ K) between nearest neighbor Mn ($\mu_{\rm Mn} = 5/2$) and NITR radicals ($\mu_{\rm NITR} = 1/2$), the long range anisotropic dipolar coupling between all species of magnetic atoms, as well as a local anisotropy on the manganese sites. The detail of the calculations are reported in the Appendix.

The role of dipolar interactions was first tested by neglecting the single-ion anisotropy term, $D = 0$. The resulting antiferromagnetic LRO was found with the propagation vector $\boldsymbol{k}$=0, as observed experimentally. However, contrary to the anisotropy inferred from neutron scattering and magnetometry measurements, the spin orientation was found along the a axis, i.e. perpendicular to the chain direction. Consequently, the influence of the single-ion anisotropy was evaluated by introducing a local uniaxial anisotropy $D > 0$ whose value was increased progressively. As results, the antiferromagnetic structure with $\boldsymbol{k}$=0 remains for all D values, but the spins direction switches to the b axis for $D/k_{\rm B}$ values greater than ≈ 160 mK. This is larger but of the same order of magnitude than the value, $D/k_{\rm B} \approx 40$ mK, estimated from the anisotropy constant K obtained via the low temperature magnetization measurements[37]. Note that due to some approximations made in the calculations (the interchain exchange coupling and the small canting with respect to the b axis were not taken into account for instance) the results should be considered as qualitative only.

These results indicate first that the dipolar interaction cannot explain the anisotropy observed in the chain, contrary to the case of other Mn-NITR chains[9]. Other mechanisms must then be invoked such as antisymmetric exchange or Mn^{2+} single-ion anisotropy. In support of this last explanation, let us note that, although often negligible, large zero field splittings have been reported in the $Cs_2MnCl_4.2H_20$ antiferromagnet ($|D/k_{\rm B}| \sim$140 mK)[38] for instance and in several Mn(II) organic compounds ($|D/k_{\rm B}|$ up to $\sim$1 K)[39]. The single-ion anisotropy has also been proposed to be the main source of anisotropy in other Mn(II) chain compounds[11,40]. In fact, one of these compounds undergoes a transition towards an antiferromagnetic LRO and is one of the rare example with the direction of the Mn moments along the chain axis[40].

The second important result of these MF calculations is that the interchain dipolar interaction produces a 3D antiferromagnetic LRO with propagation vector $\boldsymbol{k}$=0, which is robust with respect to the spins orientation. This interaction is therefore most probably responsible for the antiferromagnetic LRO observed in $Mn(hfac)_2(R)$-3MLNN below T_c.

Nevertheless, it seems difficult to reconcile the amplitude of the dipolar interaction between two spins in neighboring chains, d_{nn}, and the critical temperature:

$d_{nn} = (\mu_0/4\pi)\,(g\mu_B)^2\,/\,r_{nn}^3 \approx 1.7$ mK, for a nearest neighbor chain distance of $r_{nn} = 11.33$ Å, which is three orders of magnitude smaller than T_c=3 K.

As shown below, this apparent contradiction can be resolved as soon as one considers the intrachain correlations developing at low temperatures, which build super spins made of a temperature dependent number of strongly correlated individual spins.

The critical temperature can be calculated in a mean field approach, considering only intrachain exchange and interchain dipolar interaction. To describe the low temperature behavior of quantum-classical ferrimagnetic chains in the Heisenberg model, let us consider a single chain as independent quasi-rigid blocks, or super spins, of length ξ and total moment $\tilde{S} = \xi S_{tot}$ with $S_{tot} = S - s = 2$ (S=5/2 and s=1/2). The correlation length is then $\xi = |\tilde{J}|/2k_BT$ with $\tilde{J} = JSs$ (J/k_B=-510 K the intrachain correlation)[41].

As we know from experiments that these super spins tend to align along the b axis of the crystal, we end up with an effective model of pseudo Ising super spins $\tilde{S}$ distributed on a distorted triangular lattice and interacting via the dipolar interaction. Using d_{nn}/k_B=1.7 mK in the previously introduced formalism, the mean-field critical temperature is given by

$$T_c^{\mathrm{MF}} = \frac{c}{k_B}\, d_{nn}\tilde{S}^2/n = \frac{c}{k_B}\, d_{nn}(\xi(T_c)S_{tot})^2/n \qquad (4)$$

where $n = 3$ is the spin dimension and $c \approx 1.9$ is a dimensionless constant dependent on the two dimensional super spin lattice geometry. This finally leads to :

$$T_c^{\mathrm{MF}} = \frac{1}{k_B}\left(\frac{c}{4n}\, d_{nn}\, S_{tot}^2\, |\tilde{J}|^2\right)^{1/3} \qquad (5)$$

from which we obtain $T_c^{\mathrm{MF}} \simeq 7.6$ K. Keeping in mind that the mean field approach always tends to overestimate the transition temperature, this result seems in rather good agreement with the measured $T_c = 3$ K. Perhaps even more important is that this calculation establishes that the LRO is driven both by the intrachain exchange interaction which operates first and builds mesoscopic super spins (at T_c^{MF}, around 80 spins are strongly correlated) and by the dipolar interchain interaction which settles the 3D ordering temperature of these super spins.

As argued, the dipolar interaction should be responsible for the 3D antiferromagnetic stacking of the chains. Consequently, it cannot explain the 3D ferromagnetic correlations observed above T_c. These correlations must then be induced by the interchain exchange interaction in spite of the large interchain distances. Indeed, although short-range in nature, the exchange interaction in molecular compounds can be mediated by the spin delocalization and polarization processes on the whole NITR molecule (not only on the two O-N bridges of the radical) and between several molecules[34]. In the present structure, some C-H$\cdots$O interchain paths of lentgh 2.7 Å can be identified, which fall within the range of weak hydrogen bonds[42]. Hydrogen bonds have been shown to be possible exchange paths between molecules[43]. Such exchange mechanism should lead to a small value of the interaction energy, which is consistent with the value of the interchain exchange obtained from the mean field approach ($J_{inter}/k_B \approx$ 4 mK, see Section II) and of the same order as the dipolar energy. However, the sign of this interaction cannot be simply deduced from structural consideration due to the complexity of the exchange paths. Note that previous magnetization measurements under pressure on Mn(hfac)$_2$(R)-3MLNN also concluded the existence of ferromagnetic interchain exchange[44]. Polarized neutron experiments on a single-crystal could give more information on these interactions.

The unusual transition revealed by these experiments (ferromagnetic-like susceptibility and antiferromagnetic LRO) could therefore result from the competition between the ferromagnetic interchain exchange and the antiferromagnetic dipolar interaction, and from their different sensitivity to the strong 1D magnetic behavior. Decreasing the temperature leads to the formation within the chains of correlated blocks of spins whose length ξ increases like the inverse of the temperature. The long-range nature of the dipolar interaction makes it more sensitive to the intrachain correlations than the exchange interaction[21]. This is reflected by the transition temperature obtained in a mean field approach: T_c increases like ξ for the exchange interaction[45], whereas it increases like ξ^2 for the dipolar one (Eq. 4). Therefore, below a certain temperature, when ξ reaches a threshold value, the dominant exchange interaction leading to ferromagnetic interchain correlations can be overwhelmed by the dipolar one. This in turn should favor antiferromagnetic interchain arrangements.

This interpretation of the magnetic properties of the Mn(hfac)$_2$(R)-3MLNN compound in terms of competition between weak exchange and dipolar interactions is supported by the magnetic behavior under weak magnetic fields. In the M(H) curves (see Section II), a small curvature appears at fields of a few Oe and the intensity of magnetic Bragg peaks associated with the antiferromagnetic order starts to decrease under the same field of a few Oe (see Section III). These observations are the signature of a fast deterioration of the zero-field antiferromagnetic ground state in favor of a ferromagnetic LRO under a small field. They are consistent with the estimated strength of the antiferromagnetic dipolar interchain interaction which leads to an equivalent field of a few Oe. This transition is however not characterized by an abrupt metamagnetic transition. This could be explained by a distribution of the intrachain correlation lengths ξ, which is especially relevant in such compounds due to the finite size of the chains[46]. Because of the particular sensitivity of the dipolar interaction to the correlation length, a distribution of the ξ values would result in a distribution of the reversal fields instead of a unique field characteristic of a well-defined metamagnetic tran-

sition.

It is interesting to note a problem reported in some previously studied Mn-NITR chains[47] were ferromagnetic LRO was inferred from magnetization measurements, in contradiction to dipolar coupling calculations on the same compounds that predicted an antiferromagnetic structure. Furthermore, the calculations showed that ferromagnetic LRO could only be stabilized in magnetic fields higher than 20 Oe. In the present study, we measured similar ferromagnetic signatures by magnetometry and in addition, established the antiferromagnetic nature of the LRO by neutron diffraction. The above analysis provides a scenario for the coexistence of these two types of fluctuations and suggests that the temperature ranges where each one dominates is driven by the intrachain correlation length.

V. CONCLUSION

Magnetization measurements on the Mn-free radical chiral chain Mn(hfac)$_2$(R)-3MLNN compound have shown ferromagnetic correlations and a magnetic phase transition at T_c =3 K, but with a puzzling behavior in the ordered regime. Neutron measurements allowed to solve this intringuing problem.

In the present paper, the resolution of the magnetic structure of this compound from single-crystal neutron diffraction measurements was obtained using specific methods of analysis (rigid blocks refinement, symmetry analysis, "molecular" magnetic form factors) in order to overcome (i) the weakness of the signal and the fast deterioration of this small and brittle molecular sample and (ii) the presence of delocalized spins on the organic free radicals. Under moderate fields (H>150 Oe), the existence of a ferromagnetic LRO, evidenced by macroscopic magnetostatic studies, is confirmed. However in zero magnetic field, the actual magnetic LRO stabilized below T_c is found to be an antiferromagnetic arrangement of canted ferromagnetic chains in contrast with the ferromagnetic 3D fluctuations observed above T_c.

This result demonstrates that two types of weak interchain interactions, of opposite signs, are in competition in this compound. As shown by mean-field calculations, the dipolar one, enhanced by the intrachain spin correlations, dominates below T$_c$ and leads to an interchain antiferromagnetic structure that rapidly vanishes under weak magnetic field. The weak exchange interaction is mainly influent above T$_c$ producing strong ferromagnetic 3D correlations, a ferromagnetic LRO being only field-induced below T$_c$.

These results underline the need, in the field of molecular magnetism where weakly competing processes may be active, of using both macroscopic magnetization measurements *and* microscopic probes such as neutron diffraction.

Acknowledgments

P. Wolfers is acknowledged for his help in implementing new developments of his MXD program for handling rigid block refinement. We thank A. Sulpice for his high temperature magnetization measurements and B. Grenier for her help during the neutron diffraction experiments. This work has been supported in part by the European Commission under the Network of Excellence MAGMANet (contract 515767-2), by the Ministerio de Educación y Ciencia (Spain), under the project MAT2003-04699 and the project ejeC-Consolider CTQ2006-06333/BQU, and by Generalitat de Catalunya (2005SGR00362). Support from the Région Rhône-Alpes through the "Programme de Recherche Thématiques Prioritaires" is also gratefully acknowledged.

APPENDIX A: MEAN FIELD CALCULATIONS

For the mean field calculations[36] of the magnetic configuration selected at low temperature in presence of intrachain exchange interaction, dipolar interaction and single-ion anisotropy, we introduce the general anisotropic Hamiltonian, $\mathcal{H}$:

$$\mathcal{H} = -\frac{1}{2}\sum_{i,j}\sum_{m,n}\sum_{\alpha,\beta}\mathcal{J}\left(R_{ij}^{mn}\right)^{\alpha\beta}\mu_i^{m,\alpha}\mu_j^{n,\beta} - D\sum_{(i,m)\equiv \mathrm{Mn}}\mu_i^{m,z\,2}, \tag{A1}$$

where

$$\mathcal{J}\left(R_{ij}^{mn}\right)^{\alpha\beta} = J\delta_{R_{ij}^{mn},r_{nn}}\,(\hat{n}^{\alpha}\cdot\hat{n}^{\beta}) - d_{nn}\,\mu_i^n\,\mu_j^m\left(\frac{(\hat{n}^{\alpha}\cdot\hat{n}^{\beta})}{|R_{ij}^{mn}|^3} - \frac{3(\hat{n}^{\alpha}\cdot R_{ij}^{mn})(\hat{n}^{\beta}\cdot R_{ij}^{mn})}{|R_{ij}^{mn}|^5}\right). \tag{A2}$$

In the notation of this general model, the moment vectors are represented by $\boldsymbol{\mu}_i^m = \mu_i^m(\hat{n}^{(x)}S_i^{m,x} + \hat{n}^{(y)}S_i^{m,y} + \hat{n}^{(z)}S_i^{m,z})$, where the unit vectors $\hat{n}^{\alpha}$ are the global Cartesian unit vectors, and $S_i^{m,\alpha}$ is the α-th component of a unitary spin[48]. μ_i^m is the moment of the atom residing at site (i,m). J is the nearest neighbor exchange interaction ($J<0$ for an antiferromagnet), r_{nn} the nearest neighbor distance, D the anisotropy, taken as uniaxial for simplicity and d_{nn} the nearest neighbor dipolar coupling,

$$d_{nn} = \frac{\mu_0}{4\pi}\frac{(g\mu_{\mathrm{B}})^2}{r_{nn}^3}$$

Two indices are needed to localize a site as we describe the lattice as a Bravais lattice with eight sites per unit cell. It must be noted that the sum in Eq. A1 does not include terms with $\boldsymbol{R}_{ij}^{mn}=0$ and that in Eq. A2, positions $\boldsymbol{R}_{ij}^{mn}$ are taken in units of r_{nn}.

Before writing the mean-field free energy, the Hamiltonian is first rewritten in reciprocal space using the following transformations,

$$S_i^{m,\alpha} = \frac{1}{\sqrt{N}} \sum_{\boldsymbol{q}} S_{\boldsymbol{q}}^{m,\alpha}\, e^{-\imath \boldsymbol{q}\cdot\boldsymbol{R}_i^m}, \tag{A3}$$

$$\mathcal{J}\left(R_{ij}^{mn}\right)^{\alpha\beta} = \frac{1}{N} \sum_{\boldsymbol{q}} \mathcal{J}_{mn}^{\alpha\beta}(\boldsymbol{q})\, e^{\imath \boldsymbol{q}\cdot\boldsymbol{R}_{ij}^{mn}}, \tag{A4}$$

where N is the number of Bravais lattice points. Because we deal with a non Bravais lattice, which is moreover non centro symmetric, the resulting interaction matrix $\mathcal{J}(\boldsymbol{q})$ is a 24×24 non diagonal hermitian matrix. Hence, to completely diagonalize $\mathcal{J}(\boldsymbol{q})$ one must transform the $\boldsymbol{q}$-dependent variables, $\boldsymbol{S}_{\boldsymbol{q}}^m$, to normal mode variables. In component form, the normal mode transformation is given by

$$S_{\boldsymbol{q}}^{n,\alpha} = \sum_{p=1}^{8}\sum_{\gamma=1}^{3} U_{n,p}^{\alpha,\gamma}(\boldsymbol{q})\phi_{\boldsymbol{q}}^{p,\gamma}, \tag{A5}$$

where the indices (p,γ) label the normal modes (24 for Heisenberg spins), and $\{\phi_{\boldsymbol{q}}^{p,\gamma}\}$ are the amplitudes of these normal modes. $U(\boldsymbol{q})$ is the unitary matrix that diagonalizes $\mathcal{J}(\boldsymbol{q})$ with eigenvalues $\lambda(\boldsymbol{q})$. Finally, the mean-field free energy to quadratic order in the normal modes reads, up to an irrelevant constant,

$$\mathcal{F}(T) = \frac{1}{2}\sum_{\boldsymbol{q},p,\gamma} (nT - \lambda_p^{\gamma}(\boldsymbol{q}))|\phi_{\boldsymbol{q}}^{p,\gamma}|^2, \tag{A6}$$

where $\mathcal{F}(T)$ is the mean-field free energy per unit cell, T is the temperature in units of k_{B}, and $n=3$ for Heisenberg spins.

Therefore, the mean-field critical temperature is given by

$$T_c^{\mathrm{MF}} = \frac{1}{n}\mathrm{max}_{p,\gamma,\boldsymbol{q}}\left(\lambda_p^{\gamma}(\boldsymbol{q})\right)$$

where the corresponding wave vector $\boldsymbol{q}_{\mathrm{ord}}$ defines the magnetic propagation vector $\boldsymbol{k}$. If the extremal eigenvalue is non degenerate (which is always the case in this study), the inner structure of the magnetic unit cell is given by the corresponding eigenvector $\boldsymbol{U}_p^{\gamma}(\boldsymbol{q}_{\mathrm{ord}})$.

The main technical difficulty arises because the interaction matrix is obtained from a sum which is conditionally convergent due to the long range interaction of the dipolar coupling. The usual method to overcome this difficulty is to use the Ewald's method[49]. It appeared that this is not necessary in the present case. Whatever the truncation radius we took, as soon as it is large enough[50], we found that the ordering wave vector is always stable and that there were only slight modifications on the corresponding eigenvector. We therefore restricted ourselves to a finite sum in direct space.

* Corresponding author: virginie.simonet@grenoble.cnrs.fr

[1] M. Tamura, Y. Nakazawa, D. Shiomi, K. Nozawa, Y. Hosokoshi, M. Ishikawa, M. Takahashi, and M. Kinoshita, Chem. Phys. Lett. **186**, 401 (1991).

[2] J. P. Renard, M. Verdaguer, L. P. Regnault, W. A. C. Erkelens, J. Rossat-Mignot, J. Ribas, W. G. Stirling, and C. Vettier, J. Appl. Phys. **63**, 3538 (1988).

[3] L. Thomas, F. Lionti, R. Ballou, R. Sessoli, D. Gatteschi,and B. Barbara, Nature **383**, 145 (1996).

[4] W. Wernsdorfer and R. Sessoli, Science **284**, 133 (1999).

[5] M. Verdaguer, A. Gleizes, J. P. Renard, and J. Seiden, Phys. Rev. B **29**, 5144 (1984).

[6] O. Kahn, in *Molecular Magnetism*, (Wiley-VCH 1993).

[7] (a) A. Caneschi, D. Gatteschi, J. Laugier, and P. Rey, J. Am. Chem. Soc. **109**, 2191 (1987); (b) C. I. Cabello, A. Caneschi, R. L. Carlin, D. Gatteschi, P. Rey, and R. Sessoli, Inorg. Chem. **29**, 2582 (1990).

[8] A. Caneschi, D. Gatteschi, J. P. Renard, P. Rey, and R. Sessoli, Inorg. Chem. **28**, 2940 (1989).

[9] (a) A. Caneschi, D. Gatteschi, P. Rey, R. Sessoli, Inorg. Chem. **27**, 1756 (1988); (b) A. Caneschi, D. Gatteschi, J. P. Renard, P. Rey, and R. Sessoli, Inorg. Chem., **28** 3314 (1989); (c) A. Caneschi, D. Gatteschi, P. Rey, and R. Sessoli, Inorg. Chem. **30**, 3936 (1991).

[10] A. Caneschi, D. Gatteschi, N. Lalioti, R. Sessoli, L. Sorace, V. Tangoulis, and A. Vindigni, Chem. Eur. J. **8**, 286 (2002).

[11] (a) K. Fegy, D. Luneau, E. Belorizky, M. Novac, J.-L. Tholence, C. Paulsen, T. Ohm and P. Rey, Inorg. Chem. **37**, 4524 (1998); (b) D. Luneau and P. Rey, Coord. Chem. Rev. **249**, 2591 (2005).

[12] D. Luneau, C. Stroh, J. Cano and R. Ziessel, Inorg. Chem. **44**, 633 (2005).

[13] A. Caneschi, D. Gatteschi, N. Lalioti, C. Sangregorio, R. Sessoli, G. Venturi, A. Vindigni, A. Rettori, M. G. Pini, and M. A. Novak, Europhys. Lett. **58**, 771 (2002).

[14] C. Coulon, R. Clérac, L. Lecren, W. Wernsdorfer, and H. Miyasaka, Phys. Rev. B **69**, 132408 (2004).

[15] W. Wernsdorfer, R. Clérac, C. Coulon, L. Lecren, and H. Miyasaka, Phys. Rev. Lett. **95**, 237203 (2005).

[16] R. J. Glauber, J. Math. Phys. **4**, 294 (1963).

[17] A. Zheludev, V. Barone, M. Bonnet, B. Delley, A. Grand, E. Ressouche, P. Rey, R. Subra, and J. Schweizer, J. Am. Chem. Soc. **116**, 2019 (1994).

[18] (a) M. Minguet, D. Luneau, E. Lhotel, V. Villar, C. Paulsen, D. B. Amabilino, and J. Veciana, Angew. Chem. Int. Ed. **41**, 586 (2002); (b) M. Minguet, D. Luneau, C. Paulsen, E. Lhotel, A. Gorski, J. Waluk, D. B. Amabilino, and J. Veciana, Polyhedron **22**, 2349 (2003).

[19] L. R. Walker, R. E. Dietz, K. Andres, and S. Darack, Sol. State. Comm. **11**, 593 (1972).

[20] C. M. Wynn, M. A. Gîrtu, W. B. Brinckerhoff, K. -I. Sug-

iura, J. S. Miller, and A. J. Epstein, Chem. Mater. **9**, 2156 (1997).
[21] S. Ostrovsky, W. Haase, M. Drillon, and P. Panissod, Phys. Rev. B **64**, 134418 (2001).
[22] A. Morello, F. L. Mettes, F. Luis, J. F. Fernández, J. Krzystek, G. Aromí, G. Christou, and L. J. deJongh, Phys. Rev. Lett. **90**, 017206 (2003).
[23] M. Evangelisti, A. Candini, A. Ghirri, M. Affronte, G. W. Powell, I. A. Gass, P. A. Wood, S. Parsons, E. K. Brechin, D. Collison, and S. L. Heath, Phys. Rev. Lett. **97**, 167202 (2006).
[24] J. Seiden, J. Phys. **44**, L947 (1983).
[25] This value obtained using the Seiden model[24] has been refined compared to ref. 18 thanks to more precise measurements.
[26] F. Suzuki, N. Shibata, and C. Ishii, J. Phys. Soc. Jap. **63**, 1539 (1994).
[27] J. Vidal-Gancedo, M. Minguet, D. Luneau, D. B. Amabilino, and J. Veciana, J. Phys. Chem. Sol. **65**, 723 (2004).
[28] D. J. Scalapino, Y. Imry, and P. Pincus, Phys. Rev. B **11**, 2042 (1975).
[29] H. E. Stanley, in *Introduction to phase transitions and critical phenomena* (Oxford University Press, 1971).
[30] M. S. Lehmann and F. K. Larsen, Acta Crystallogr. **B26**, 1198 (1970).
[31] P. J. Brown and J. C. Matthewman, *The Cambridge Crystallographic Subroutine Library*, **RL-81-063**.
[32] P. Wolfers, J. Appl. Cryst **23**, 554 (1990).
[33] O. V. Kovalev, in *Representation of the Crystallographic Space groups, Irreducible Representations, Induced Representations and Corepresentations*, 2nd ed. (Gordon and Breach Science Publishers, Amsterdam, 1993).
[34] J. Schweizer and E. Ressouche in *Magnetism: Molecules to Materials*, edited by J. S. Miller and M. Drillon (Wiley-VCH, 2000), p. 325-355.
[35] A. Edgar, E. Siegel, and W. Urban, J. Phys. C:Solid St. Phys. **13**, 6649 (1980).
[36] M. Enjalran and M. J. P. Gingras, Phys. Rev. B **70**, 174426 (2004).
[37] The D value is calculated for single-ion anisotropy on the Mn site only, whereas the D estimated from the measurements is derived for a model of S_{tot}=2 magnetic entities. These values are therefore not directly comparable but should be in qualitative agreement.
[38] T. Smith and S. A. Friedberg, Phys. Rev. **177**, 1012 (1969).
[39] (a) W. B. Lynch, R. S. Boorse, and J. H. Freed, J. Am. Chem. Soc. **115**, 10909 (1993); (b) R. M. Wood, D. M. Stucker, L. M. Jones, W. B. Lynch, S. K. Misra, and J. H. Freed, Inorg. Chem. **38**, 5384 (1999); (c) S. K. Smoukov, J. Tesler, B. A. Bernat, C. L. Rife, R. N. Armstrong, and B. M. Hoffman, J. Am. Chem. Soc. **124**, 2318 (2002).
[40] T. Smith and S. A. Friedberg, Phys. Rev. **176**, 660 (1968).
[41] J. Curély and R. Georges, J. Phys. I France **5**, 485 (1995).
[42] J. L. Alonso, S. Antolínez, S. Blanco, A. Lesarri, J. C. López, and W. Caminati, J. Am. Chem. Soc. **126**, 3244 (2004).
[43] F. M. Romero, R. Ziessel, M. Bonnet, Y. Pontillon, E. Ressouche, J. Schweizer, B. Delley, A. Grand, and C. Paulsen, J. Am. Chem. Soc. **122**, 1298 (2000).
[44] V. Laukhin, B. Martínez, J. Fontcuberta, D. B. Amabilino, M. Minguet, and J. Veciana, J. Phys. Chem. B **108**, 18441 (2004).
[45] J. Villain and J. M. Loveluck, J. Phys. Lett. **38**, 510 (1977).
[46] L. Bogani, A. Caneschi, M. Fedi, D. Gatteschi, M. Massi, M. A. Novak, M. G. Pini, A. Rettori, R. Sessoli, and A. Vindigni, Phys. Rev. Lett. **92**, 207204 (2004).
[47] A. Caneschi, D. Gatteschi, and A. le Lirzin, J. Mater. Chem. **4**, 319 (1994).
[48] Note that the dipolar term in $\mathcal{H}$ was computed with either a localized spin 1/2 on the NITR average position or with fractions of spin on both N-O fragments of the NITR in order to take into account the delocalizion of the spin. Similar results were found in both calculations.
[49] P. P. Ewald, Ann. Phys. (Leipzig) 64, 253 (1921).
[50] Beyond a truncation radius of 300 times the nearest neighbor distance, even the eigenvector modifications are not noticeable, e.g, lower than 10^{-2} for a normalized eigenvector.